machines

MDPI

Article

Vibration Fatigue Characteristics of a High-Speed Train Bogie and Traction Motor Based on Field Measurement and Spectrum Synthesis

Lirong Guo [1], Guoshun Li [1,*], Can Chen [1,2], Yichao Zhang [1], Hongwei Zhang [1] and Dao Gong [3,*]

[1] Locomotive & Car Research Institute, China Academy of Railway Sciences Corporation Limited, Beijing 100081, China; guolirong@rails.cn (L.G.); chencan@rails.cn (C.C.); zhangyichao@rails.cn (Y.Z.); zhanghongwei@rails.cn (H.Z.)
[2] School of Mechanical, Electronic and Control Engineering, Beijing Jiaotong University, Beijing 100044, China
[3] Shanghai Key Laboratory of Rail Infrastructure Durability and System Safety, College of Transportation, Tongji University, Shanghai 201804, China
* Correspondence: liguoshun@rails.cn (G.L.); gongdao@tongji.edu.cn (D.G.)

Abstract

In this study, the fatigue behavior in high-speed train bogie frames and mounted traction motors was investigated through dynamic stress measurements and vibration analysis. A spectrum synthesis method was developed to integrate multipoint random vibrations from the bogie frame into a unified excitation spectrum for motor fatigue assessment. The results demonstrate that fatigue damage in the bogie frame progresses linearly with increasing speed, with critical stress concentrations being identified at the motor base weld seams (41.4 MPa equivalent stress at 400 km/h). Traction motor vibration spectra were found to deviate substantially from IEC 61373 standards, leading to higher fatigue damage that follows an exponential growth pattern relative to speed increases. The proposed methodology provides direct experimental validation of component-specific fatigue mechanisms under operational loading conditions.

Keywords: high-speed vehicle; bogie frame; traction motor; spectrum synthesis; vibration environment spectrum; fatigue analysis

check for updates

Academic Editor: Ciro Santus

Received: 18 June 2025
Revised: 14 July 2025
Accepted: 15 July 2025
Published: 16 July 2025

Citation: Guo, L.; Li, G.; Chen, C.; Zhang, Y.; Zhang, H.; Gong, D. Vibration Fatigue Characteristics of a High-Speed Train Bogie and Traction Motor Based on Field Measurement and Spectrum Synthesis. *Machines* **2025**, *13*, 613. https://doi.org/10.3390/machines13070613

Correction Statement: This article has been republished with a minor change. The change does not affect the scientific content of the article and further details are available within the backmatter of the website version of this article.

Copyright: © 2025 by the authors. Licensee MDPI, Basel, Switzerland. This article is an open access article distributed under the terms and conditions of the Creative Commons Attribution (CC BY) license (https://creativecommons.org/licenses/by/4.0/).

1. Introduction

Railway trains are transitioning toward higher speeds to better support national economic development. However, this transition leads to more pronounced vibrations in vehicle components, potentially leading to fatigue failure. Among the critical components of railway trains, bogies are particularly prone to fatigue failure due to their role as the main load-bearing structure. The safety and reliability of the vehicle bogie are therefore key to ensuring operational safety.

The fatigue strength of the bogie frame of railway vehicles has been analyzed extensively using numerical methods. Kim et al. [1] investigated the strength evaluation procedure of a bogie frame for tilting railway vehicles. They derived the loading conditions imposed on the tilting train and evaluated the static and fatigue strength of the bogie frame using multi-body dynamic analyses and finite element analysis (FEA). The results of this study aided in ensuring the structural safety of the bogie frame. Seo et al. [2] conducted a fatigue design evaluation of a railway bogie frame through full-scale fatigue testing. Strength analysis was performed using FEA to identify stress concentration areas. Dynamic

stress was measured using strain gauges, revealing multiaxial loading conditions. Fatigue strength evaluations were then conducted by employing a critical plane approach. Kraus et al. [3] conducted a study on the development of bogie frames for rail vehicles from a strength and fatigue life perspective. The development process included stress calculations, static and fatigue tests, and validation of fatigue life data through stress monitoring during test runs on an actual track. Ji et al. [4] developed a virtual track irregularity (VTI) and simplified dynamics model (SVDM) method for load spectrum generalization across high-speed train bogies. They found that the VTI-SVDM combination accurately predicts frame-specific load histories, enabling reliable cross-configuration load transfer while preserving damage equivalence in bogie frame assessments. Yang et al. [5] demonstrated in their study that the semi-active inertial suspension effectively improves vibration isolation and minimizes fatigue-induced performance losses over the entire frequency spectrum. In another study, Yamazaki et al. [6] proposed a fatigue assessment method for bogie frames by estimating dynamic stresses through finite element analysis using axle box acceleration data, enabling fatigue life prediction and damage visualization across the entire structure. Han et al. [7] developed a 3D rigid–flexible coupling model of a high-speed train, incorporating gear meshing dynamics and wheel polygonization, to assess bogie frame fatigue damage using finite element analysis and rainflow counting. Sanikhani et al. [8] developed a data-driven surrogate model using CatBoost—selected as the optimal ML algorithm among nine candidates—to assess the fatigue failure probability of bogie frames under parameter variability, achieving 99.34% reliability over 30 years while demonstrating effectiveness with limited training data. Sun et al. [9] developed a flexible multibody dynamics model incorporating wheel–rail contact nonlinearities to investigate wheel out-of-roundness (OOR)-induced bogie frame vibrations, employing modal stress recovery to analyze dynamic stresses and establish safe OOR amplitude limits through comprehensive time–frequency domain simulations. Wang et al. [10] developed an extreme value theory-based time–domain extrapolation method for the accurate fatigue life assessment of railway structures using limited short-term stress data. In the aforementioned studies, the researchers investigated the fatigue strength of vehicles using simulations. However, numerical simulation methods sometimes struggle in reproducing real service conditions. In contrast, measurement methods can aid in more accurately determining the real stress results of the bogie and are more suitable for analyzing fatigue strength.

In addition, fatigue failure of mounted components also occurs frequently, particularly for the traction motor, the mass of which is greater than that of other components [11]. These components are excited by the random vibration of the bogie frame. The quantitative expression of these vibrations is crucial for analyzing fatigue strength [12–18]. For this purpose, the International Electrotechnical Commission (IEC) published the IEC 61373 standard to define these vibration characteristics using the power spectral density (PSD) [19]. After its publication, Mu et al. [20] utilized the IEC 61373 standard to analyze the axle box. Zhang et al. [21] also utilized the IEC 61373 standard to analyze their measured data.

It should be noted, however, that the IEC 61373 standard cannot fully express the actual vibration characteristics of the bogie frame, which are non-Gaussian and non-stationary. At present, there have been few studies on the description and statistical generalization of this vibration in the railway vehicle field. Despite this, in other fields of transportation engineering, such as the aerospace and military fields, researchers have begun to study the random vibration environment of airborne equipment with a method referred to as spectrum synthesis. Jang et al. [22] refined the Damage Potential (DP) method from MIL-STD-810 for vibration fatigue analysis. While DP's simplified FDS approach works for test standard comparisons, it has limitations for vibration synthesis. This approach, when applied to generate vibration fatigue load spectra for equipment mounted on a railway

vehicle, therefore has the potential to address the limitations of the IEC 61373 standard spectrum. By using this approach, the obtained vibration spectrum can accurately quantify the vibration characteristics of the bogie frame.

In summary, analyzing the fatigue damage of the bogie frame and the mounted traction power in actual service environments plays an important role in ensuring the operational safety of vehicles. In this study, a well-prepared measurement plan is utilized to obtain the dynamic stress and vibration of the bogie frame. The developed spectrum synthetic method is utilized to generate the vibration excitation spectrum of the traction motor, in which a method for processing multipoint random vibrations from the bogie frame is proposed. Thereafter, the fatigue damage to the bogie frame and the mounted motor is analyzed with respect to the different operational speeds.

The remaining sections of this paper are organized as follows: in Section 2, the dynamic stress of the bogie frame is determined and the fatigue damage is analyzed; in Section 3, the spectrum synthesis method is proposed to generate the vibration excitation spectrum; in Section 4, the fatigue damage of the traction motor is analyzed with from these loads; lastly, the conclusion is presented in Section 5.

2. Fatigue Analysis of the Bogie Frame Based on Onsite Measured Stress

In this section, the fatigue assessment methodology employed for a high-speed train bogie frame is described, combining numerical analysis based on the UIC 615-4 standard [23] and experimental stress measurements.

2.1. Dynamic Stress Test Preparation of the Bogie Frame

The UIC 615-4 standard ("Structural Strength Test Method for Railway Passenger Cars-Trailer Bogies-Bogies and Running Devices-Bogie Frames") was utilized to calculate the stress distribution of the bogie frame. The force and working conditions defined in the UIC 615-4 standard were applied to the bogie frame, as shown in Table 1. Thereafter, the stress cloud map was obtained, in which the results from working condition number 1 are shown in Figure 1.

Based on engineering experience [24,25] and the stress cloud map, the measured position of the bogie frame was determined, including the weld seams of the mounting seats for different components and stress concentration areas, as illustrated in Figure 2.

Table 1. Calculating the condition under the simulation loads for the frame.

	Vertical Force (Left)	Vertical Force (Right)	Transverse Force
1	Fz	Fz	0
2	$(1 + \alpha - \beta)\cdot Fz$	$(1 - \alpha - \beta)\cdot Fz$	0
3	$(1 + \alpha - \beta)\cdot Fz$	$(1 - \alpha - \beta)\cdot Fz$	Fy
4	$(1 + \alpha - \beta)\cdot Fz$	$(1 - \alpha + \beta)\cdot Fz$	
5	$(1 + \alpha - \beta)\cdot Fz$	$(1 - \alpha + \beta)\cdot Fz$	Fy
6	$(1 - \alpha - \beta)\cdot Fz$	$(1 + \alpha - \beta)\cdot Fz$	
7	$(1 - \alpha - \beta)\cdot Fz$	$(1 + \alpha - \beta)\cdot Fz$	−Fy
8	$(1 - \alpha + \beta)\cdot Fz$	$(1 + \alpha + \beta)\cdot Fz$	
9	$(1 - \alpha + \beta)\cdot Fz$	$(1 + \alpha + \beta)\cdot Fz$	−Fy

Where Fz is the vertical force applied on the side beam of the bogie frame; Fy is the transverse force applied on the lateral buffer seat; β is the percentage of change in vertical force caused by the vertical motion of the car body (sinking and floating motion); α is the percentage of change in vertical force caused by the rolling of the car body. In this case, $\alpha = 0.1$ and $\beta = 0.2$.

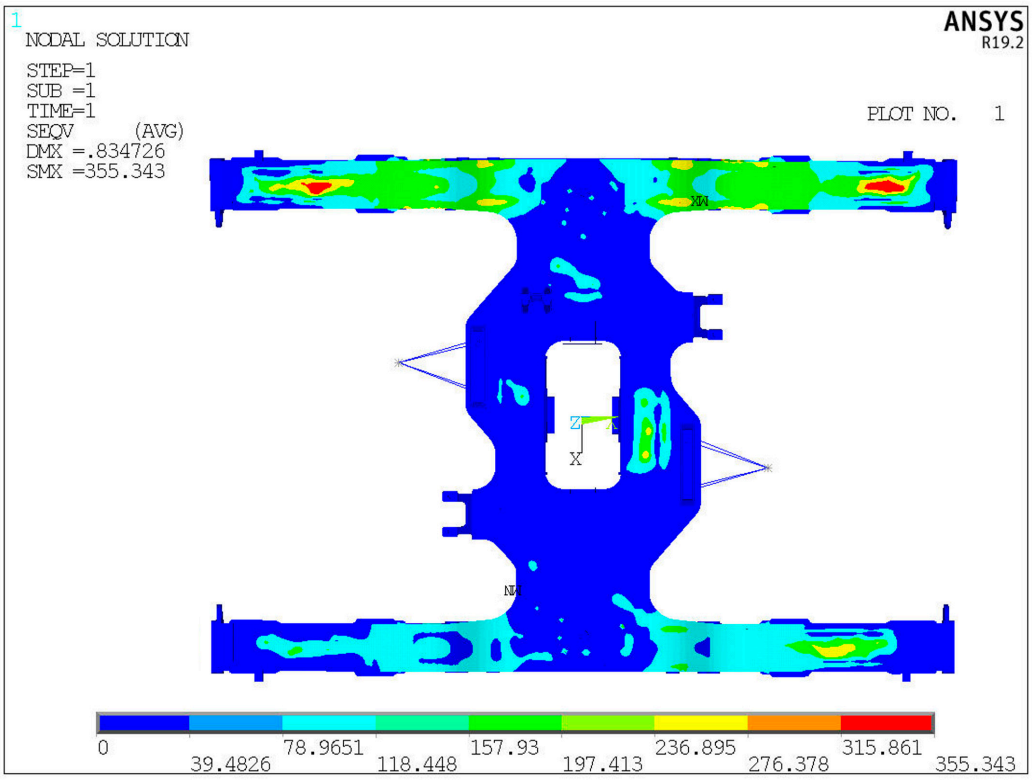
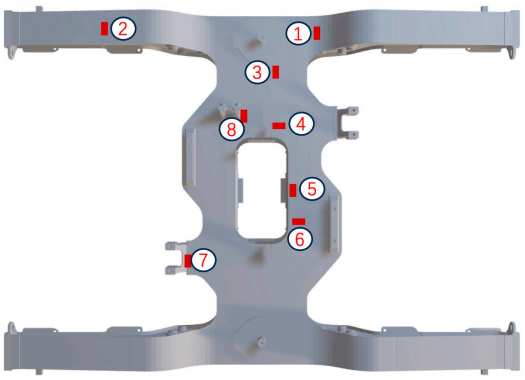


Figure 1. Schematic diagram of bogie frame stress cloud map.



① Base material of frame
② Welding seam of brake mounting seat
③ Base material of frame
④ Weld seam on lateral buffer seat
⑤ Weld seam on traction power seat
⑥ Weld seam on draw bar seat
⑦ Weld seam on gearbox seat
⑧ Weld seam on lateral damper seat

Figure 2. Scheme of the strain gauge positions.

The strain bridge assembly method shown in Figure 3 was used to measure the strain of the bogie frame of the high-speed train operating on the track line. ε_1 denotes a working strain gauge pasted onto the test structure, ε_4 denotes a temperature–compensation strain gauge, ε_2 and ε_3 denote non-working strain gauges, and ε_2, ε_3, and ε_4 are applied to the non-deformable components of materials with the same properties as the test structure. In this test, we adopted the quarter bridge method, with a strain gauge working resistance of 120 Ω, a measurement range of 0–2000, and a sensitivity coefficient of 2. In this test, eight strain gauges were used to obtain frame strain data during the operation of the train at speeds of 350, 380, and 400 km/h, with a sampling frequency of 2000 Hz. Partial measured stress data are shown in Figure 4.

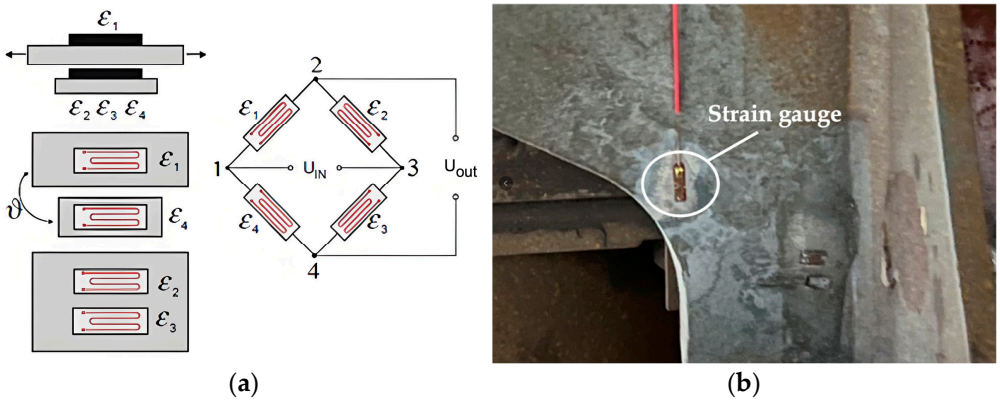


Figure 3. Strain testing on the bogie frame: (**a**) bridge assembly method for strain measurement and (**b**) field test diagram.

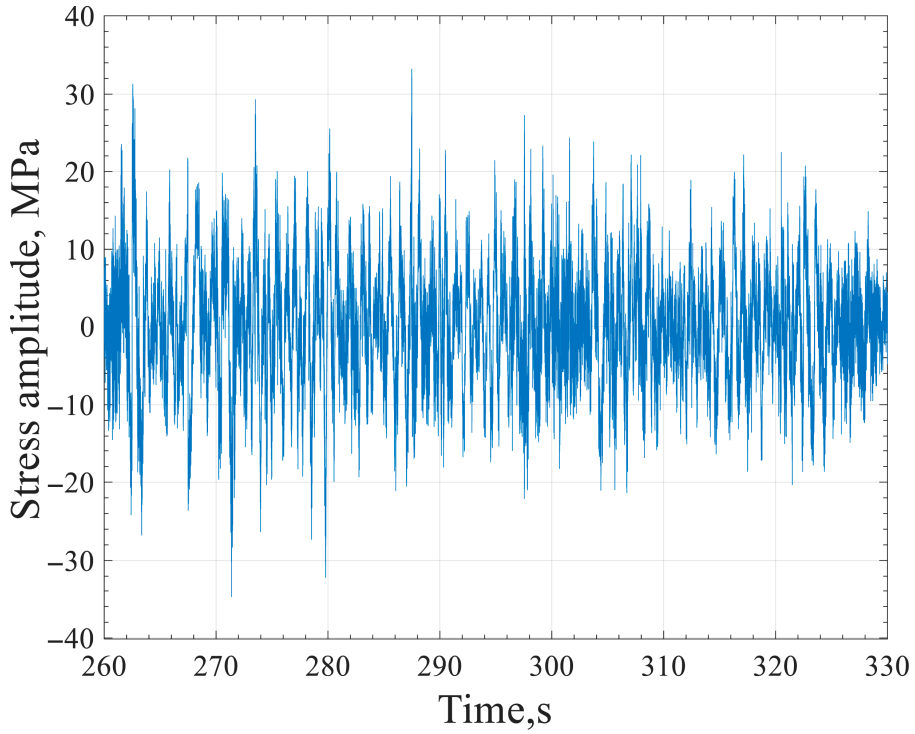


Figure 4. Measured stress.

2.2. Fatigue Analysis Method with the Measurement Stress

Based on the S-N curve, at a certain stress level,

$$\sigma_{-1}^{m} N_{-1} = \sigma_i^m N_i = C \tag{1}$$

where σ_{-1} represents the fatigue limit of the material under symmetric cyclic conditions, N_{-1} represents the number of cycles that fail when the load reaches the fatigue limit, σ_i represents the stress level, and N_i represents the number of cycles at which fatigue failure occurs at this stress level. Based on BS 7608 Fatigue Design and Evaluation of Steel Structures, for the base material, m = 3.5, σ_{-1} = 78, and for welds, m = 3, σ_{-1} = 40.

Based on Miner's linear damage accumulation rule and the material S-N curve, the obtained multilevel stress spectrum can be transformed into a single stress amplitude for a certain number of cycles under equal damage conditions, which is known as the equivalent

stress amplitude. Therefore, the expression for the structural damage D_1 corresponding to the test stress spectrum is

$$D_1 = \sum_{i=1}^{p} \frac{n_i}{N_i} = \sum_{i=1}^{p} \frac{n_i \sigma_{ai}^m}{C_1} \tag{2}$$

where N_i represents the number of cycles of the stress amplitudes at each level, C_1 and m are the parameters of the S-N curve, $\sigma_{\alpha i}$ represents the stress amplitude at each level of the stress spectrum, and P represents the stress spectrum series.

If the equivalent stress amplitude acts N times and the damage caused by the structure is D, then

$$D = \frac{N \sigma_{aeq}^m}{C_1} \tag{3}$$

where σ_{aeq}^m represents the equivalent stress amplitude, and N represents the number of cycles corresponding to the fatigue limit of the material or welded joint. For welded steel joints, $N = 2 \times 10^6$.

It is assumed that the measured stress spectrum runs for L_1 km, and the resulting damage is expressed as D_1. If the safe operating mileage that generates the cumulative damage D is L, then

$$\frac{D}{L} = \frac{D_1}{L_1} \tag{4}$$

Substituting the expressions of D and D_1 yields

$$\sigma_{aeq} = \left[\frac{L}{L_1 N} \sum n_i (\sigma_{-1ai})^m \right]^{\frac{1}{m}} \tag{5}$$

$$\frac{N \sigma_{aeq}^m}{C_1 L} = \sum \frac{n_i \sigma_{-1ai}^m}{C_1 L_1} \tag{6}$$

2.3. Fatigue of the Bogie Frame

Measurements were performed on a high-speed rolling stock bogie to obtain the dynamic stress data. In this test, eight sensors were arranged to measure the vibration load of the motor equipment during the operation of the train at speeds of 350, 380, and 400 km/h, with a sampling frequency of 2000 Hz.

As shown in the test results presented in Table 2 and Figure 5, with the increase in speed, the maximum stress at 400 km/h decreases, and the maximum stress in the remaining regions tends to increase. At 400 km/h, the maximum stress of the weld seam on the traction motor seat is the highest (41.4 MPa); in comparison, the maximum stress of the weld seam of the gearbox seat is the lowest (13.5 MPa).

Table 2. Equivalent stress amplitude value of the bogie frame.

Measurement Position	300 km/h	350 km/h	380 km/h	400 km/h
Weld seam on lateral buffer seat (MPa)	28.9	32.2	34.8	38.8
Base material of frame (MPa)	17.5	22.3	25.3	28.6
Weld seam of draw bar seat (MPa)	15.7	16.8	18	19.3
Weld seam of brake mounting seat (MPa)	13.8	15	16.9	20.6
Weld seam on traction motor seat (MPa)	34.5	37	41.1	41.4
Base material of frame (MPa)	20.1	22.3	25.3	29.8
Weld seam of gearbox seat (MPa)	10.9	11.3	12.6	13.5
Weld seam of lateral damper seat (MPa)	10.7	11.5	12.8	13.7

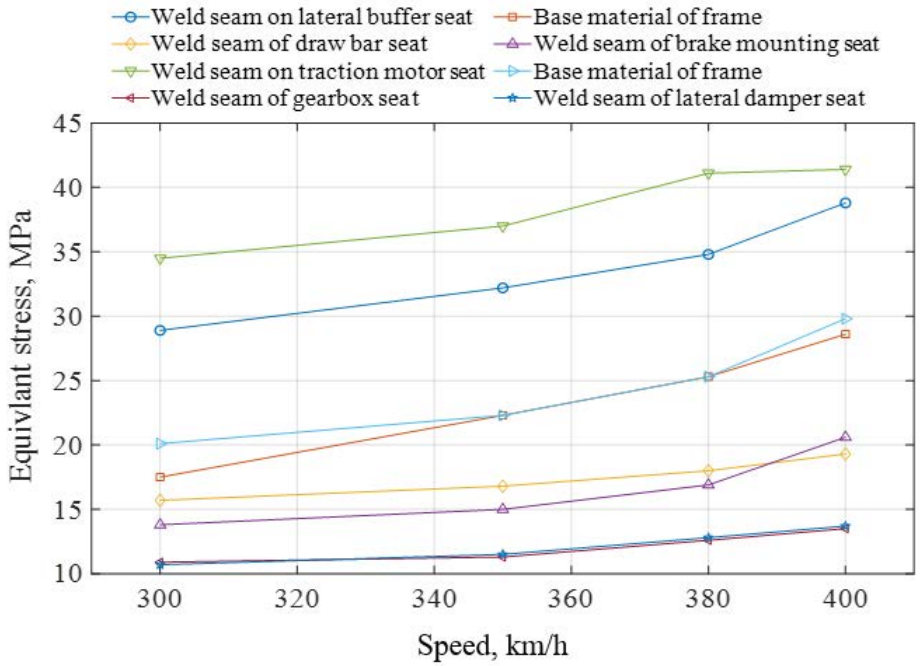


Figure 5. Equivalent stress values at measurement points of different speed levels.

3. Vibration Load of the Traction Motor

The installation seat of the traction motor bears the random vibration of the bogie frame caused by random wheel–rail unevenness during service. Analyzing these random vibrations is important for studying the vibration and fatigue of motor-installed seats. The input random vibration environment data samples were summarized, organized, and compiled into environmental spectra.

3.1. Vibration Testing at the Installation Site of the Traction Motor

Measurements were performed on a bogie motor mount to obtain the equipment vibration load data. In this test, four three-direction vibration acceleration sensors were arranged to measure the vibration load of the motor equipment during the operation of the train at speeds of 300, 350, 380, and 400 km/h, with a sampling frequency of 2000 Hz. The arrangement of the measurement points is illustrated in Figure 6. Positions 1 to 4 are the four vibration acceleration measurement points.

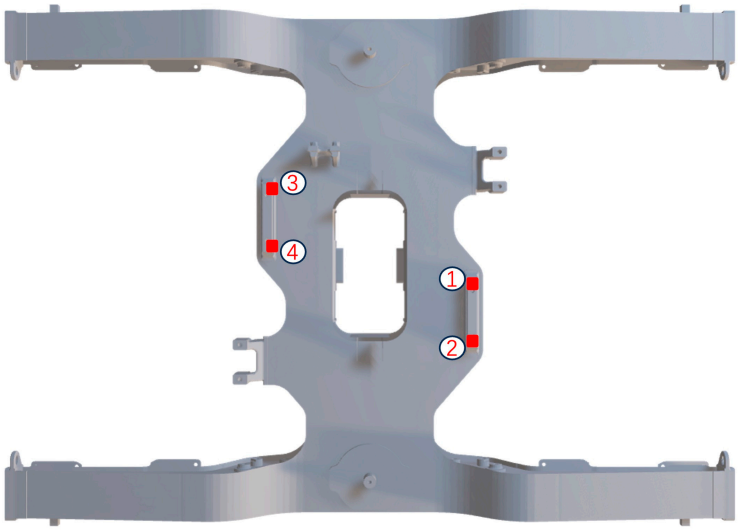


Figure 6. Field measurement for vibration of the bogie frame.

3.2. Methods for Defining Vibration Environments

The time–domain vibration acceleration data were collected from the measurement-point channels of the bogie motor (at least 20 s per segment). First, the power spectra of all of the samples were calculated and denoted as G_k (i, j) $(i = 1, 2, \ldots, L; j = 1, 2, \ldots, M; k = 1, 2, \ldots, N)$, where i represents the channel number, L represents the total number of channels, j represents the sample number, M represents the total number of samples, k represents the spectral line number, and N represents the total number of spectral lines. For the k-th dimension, we took the root mean square value of G_k (i, j) and denoted it as R (i, j).

For different channels, the mean X_i and variance S_i^2 of sequence $R(i, j)$ were estimated separately [26]:

$$\begin{cases} X_i = \dfrac{1}{M_1}\sum\limits_{j=1}^{M} R(i,j) \\ S_i^2 = \dfrac{1}{M_1 - 1}\sum\limits_{j=1}^{M} (R(i,j) - X_i)^2 \end{cases} \tag{7}$$

The a-th and b-th channels were selected, and the statistics $F(a, b)$ and $t(a, b)$ were computed using the estimated means and variances.

If the power spectra of channels a and b belong to the same general population, $F(a, b)$ obeys the F-distribution with degrees of freedom $(M - 1, M - 1)$, and $t(a, b)$ obeys the central t-distribution with degrees of freedom $2(M - 1)$, which implies that it holds for a given confidence level $1 - \alpha$. Conversely, they do not belong to the same aggregate.

$$\begin{cases} F_{\alpha/2}(M-1, M-1) \le F(a,b) \le F_{1-\alpha/2}(M-1, M-1) \\ |t(a,b)| \le t_{1-\alpha/2}(2M-2) \end{cases} \tag{8}$$

The data belonging to the same channel were grouped together to form the feature sample G_k (p, q) $(p = 1, 2, \ldots, P; q = 1, 2, \ldots, Q; k = 1, 2, \ldots, N)$, where p represents the feature channel serial number, P represents the total number of feature channels (less than or equal to the total number of channels), q represents the sample serial number, and Q_p represents the number of samples in the p-th feature channel.

The definitions are as follows:

$$x_k(p, q) = \sqrt{G_k(p, q)} \tag{9}$$

We estimated the mean $X_k(p)$ and variance $S_i^2(p)$ of sample $x_k(p, q)$, that is,

$$\begin{cases} X_k(p) = \dfrac{1}{Q_p}\sum\limits_{q=1}^{Q_p} x_k(p,q) \\ S_k^2(p) = \dfrac{1}{Q_p - 1}\sum\limits_{q=1}^{Q_p} (x_k(p,q) - X_k(p))^2 \end{cases} \tag{10}$$

Thereafter, we calculated the upper tolerance coefficient F_1 for a confidence level of $(1 - \alpha)$ and a quantile point of β, i.e., $\alpha = 0.05$, $\beta = 0.9$.

$$F_1 = \frac{t_{1-\alpha}(Q_p - 1)}{\sqrt{Q_p}} + Z_\beta \sqrt{\frac{Q_p - 1}{\chi^2{}_\alpha (Q_p - 1)}} \tag{11}$$

where Z_β is the normal quantile point satisfying $P(Z \le Z_\beta) = \beta$; ${\chi^2}_{1-\alpha/2}(Q_p - 1)$ is the χ^2 distribution α quantile point whose degree of freedom is $Q_p - 1$.

The upper tolerance limit is estimated for the p-th sample, i.e.,

$$G_k(p) = (X_k(p) + F_1 S_k(p))^2 \tag{12}$$

The above results in the measured spectrum of the random vibration of the bogie motor, i.e., $G_k(p)$.

3.3. Vibration Environment Spectrum

Based on the measured data collected from the vibration mounting seat of the bogie motor, the environment spectrum of the motor vibration at different operating speeds was compiled using the aforementioned method, which facilitated the subsequent analysis of the frequency–domain distribution characteristics. The vibration spectra of high-speed rolling stock bogie motors under different operating speeds are shown in Figures 7–9.

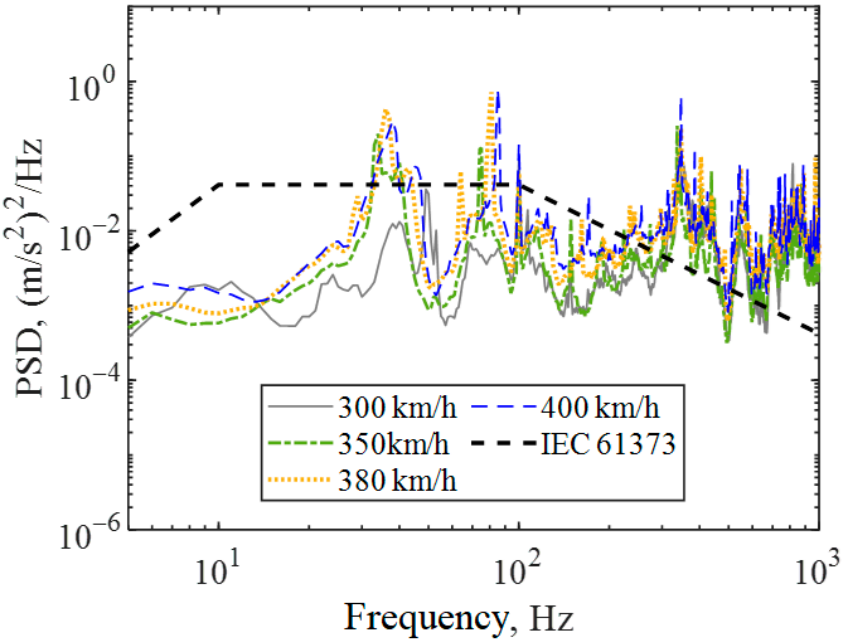


Figure 7. X-direction vibration spectra of the motor of a high-speed train at different speeds.

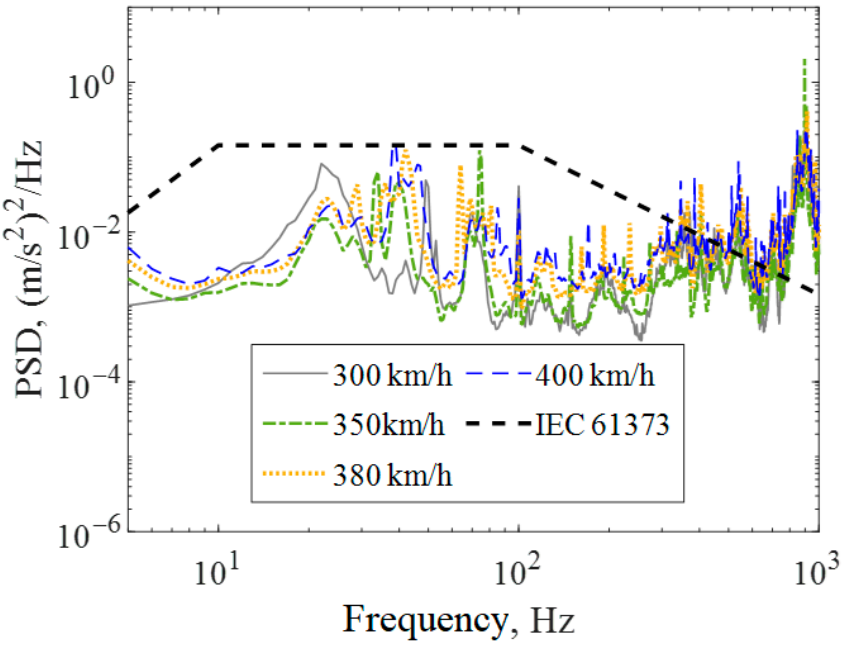


Figure 8. Y-direction vibration spectra of the motor of a high-speed train at different speeds.

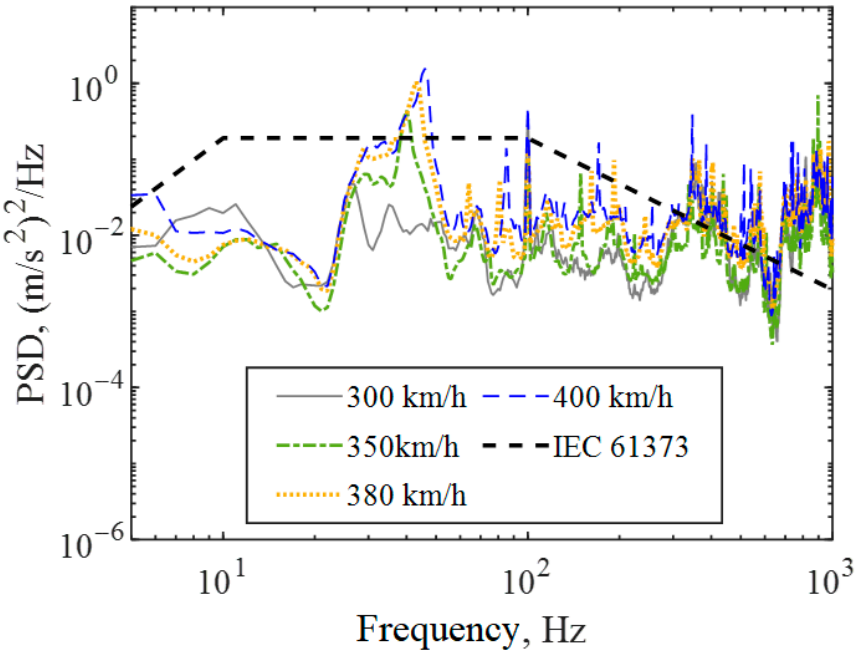


Figure 9. Z-direction vibration spectra of the motor of a high-speed train at different speeds.

At different speeds, the vibration energy values of the bogie motor vary, and the frequency–domain distribution characteristics are essentially identical; however, the peak appeared to shift to the right as the speed increased. First, in the X-direction, 300, 350, 380, and 400 km/h speeds under the bogie motor vibration energy value exhibited minimal difference at 3.5, 3.3, 4.2, and 4.4 m/s^2, respectively, in agreement with the characteristics of the energy value with the increase in speed, and were higher than the IEC standard provisions of 2.5 m/s^2. In the low-frequency band, the vibration environment spectrum value of the bogie motor was lower than the standard spectrum value, and the peak appeared to shift to the right with the increase in speed. In contrast, in the high-frequency region, the vibration environment spectrum of the bogie motor was far higher than the standard spectrum value.

In the Y-direction, 300, 350, 380, and 400 km/h speeds under the bogie motor vibration energy value exhibited minimal difference, at 4.9, 5.0, 5.3, and 5.3 m/s^2, respectively, in agreement with the idea that the energy value increases with the increase in speed, with a value slightly greater than the stipulated IEC standard of 4.7 m/s^2. In the low-frequency band, the bogie motor vibration spectral value was lower than the standard spectral value; in contrast, in the high-frequency band, the vibration spectral value of the bogie motor was significantly higher than the standard spectral value.

In the Z-direction, 300, 350, 380, and 400 km/h speeds under the bogie motor vibration energy value exhibited minimal difference, respectively, at 4.7, 4.3, 5.5, and 6.1 m/s^2, in agreement with the characteristics of the energy value increases with the increase in speed, essentially close to the IEC standard of 5.5 m/s^2. In the low-frequency band, the bogie motor vibration environment spectrum value was lower than the standard spectrum value; in the high-frequency band, in comparison, the vibration environment spectrum value was far higher than the standard spectrum value.

4. Fatigue Analysis of the Traction Motor

The fatigue performance of the traction motor is critical to ensuring the reliability of high-speed train operation. To evaluate its structural behavior under dynamic loads, a finite element model was established to enable stress and fatigue assessment.

4.1. Finite Element Model of the Traction Motor

The geometric model of the motor was imported into Hypermesh 2021 software to establish the FE model. The PSHELL elements were used to discretize the traction motor. Constraints were applied to the mounting positions to restrict displacements in longitudinal (X), transverse (Y), and vertical (Z) directions. The finite element model after discretization is shown in Figure 10, where different colors represent different components. Three progressively refined meshes (15 mm, 10 mm, and 5 mm element sizes) were evaluated, with less than 5% variation observed in maximum displacement results at the mounting positions, confirming mesh independence. All elements satisfy ASME V&V 10.1–2012 quality criteria [27].

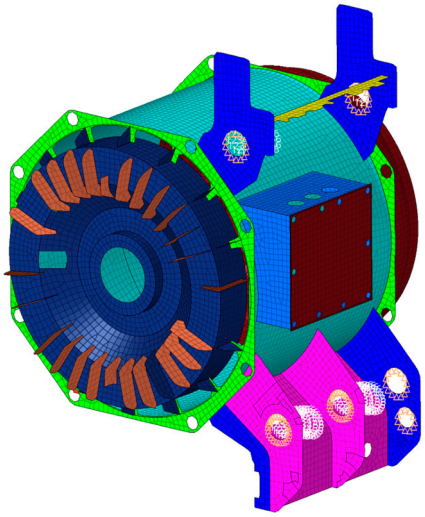


Figure 10. Finite element model of the traction motor.

Special refinement was implemented at mounting interfaces (with the element size reduced to 3 mm) to capture stress concentrations, utilizing unstructured mesh patterns in these critical regions. The final model contains 2.23 million elements, representing the cast iron material (Young's modulus = 110 GPa; Poisson's ratio = 0.3; density = 7850 kg/m^3) of the bogie frame. The total model mass converged to 175 kg, matching the physical prototype within 1.5%.

4.2. Fatigue Analysis of Traction Motors Based on UIC Standards

Based on UIC 615-4, the acceleration corresponding to the inertial load of the traction motor under operating conditions was applied according to the following principles: the longitudinal acceleration of the traction motor is $\pm$2.5 g, the lateral acceleration is $\pm$5.0 g, the vertical acceleration is $\pm$6.0 g, and the number of cycles is 10^7.

Based on the fatigue condition requirements, the motor was loaded to obtain the first principal stress under longitudinal, transverse, and vertical vibration conditions at the evaluation position. Based on the UIC standard, the allowable stress range is 40 MPa, and the curve slope m is 3. The calculation results are presented in Table 3.

Table 3. Traction motor damage.

	Longitudinal Damage	**Lateral Damage**	**Vertical Damage**	**Cumulative Damage**
Motor suspension seat	2.51×10^{-4}	3.21×10^{-2}	5.61×10^{-6}	3.26×10^{-2}

As shown in Table 2, after 1×10^7 cycles, the cumulative fatigue damage in the suspension was <1, which satisfied the fatigue–strength requirements. The fatigue damage under the lateral vibration level was significant, reaching 0.032, but remained within a safe range.

4.3. Fatigue Analysis of Traction Motors Based on Environment Spectrum

In real-world operating conditions, traction motors are subjected to complex random vibration loads that necessitate the use of spectral analysis methods for accurate fatigue evaluation. The frequency–domain approach provides an effective solution for processing these stochastic loadings through advanced cycle counting techniques.

4.3.1. Fatigue Analysis Theory in the Frequency Domain

To determine the stress response spectrum of the bogie frame motor, the Dirlik rainflow amplitude probability density function was used to calculate the number of stress cycles. The Dirlik rainflow counting method is based on the results of numerous Monte Carlo simulations and employs a purely empirical closed-form expression [28] that approximates the probability density function of the rainflow amplitude, consisting of one exponential and two Rayleigh distributions. The expressions are as follows:

$$f_{(S_a)}(S_a) = \frac{A_1}{2\sqrt{M_0}T} e^{\frac{-Z}{T}S_a} + \frac{A_2 Z}{2\sqrt{M_0}V^2} e^{\frac{-Z^2}{2V^2}S_a^2} + \frac{A_3 Z}{2\sqrt{M_0}} e^{\frac{-Z^2}{2}S_a^2} \tag{13}$$

where $Z = \frac{1}{2\sqrt{M_0}}$, $\gamma = \frac{M_2}{\sqrt{M_0 M_4}}$, $X_m = \frac{M_1}{M_0}\sqrt{\frac{M_2}{M_4}}$, $A_1 = \frac{2(X_m - \gamma^2)}{1+\gamma^2}$, $V = \frac{\gamma - X - A_1^2}{1-\gamma-A_1+A_1^2}$, $A_2 = \frac{1-\gamma-A_1+A_1^2}{1-V}$, $A_3 = 1 - A_1 - A_2$, and $T = \frac{1.25(\gamma - A_3 - A_2 V)}{A_1}$.

The one-sided stress response PSD function is defined by M_0, M_1, M_2, and M_3. With the 0th-, 1st-, 2nd-, and 4th-order moments of the stress response, then Mi is defined as follows:

$$M_i = \int_0^{+\infty} f^i W(f) df \tag{14}$$

The Dirlik fatigue damage model for the time period τ is expressed as follows:

$$D = \frac{E(P)\tau}{C} \int_0^{+\infty} S_a^m f_{S_a}(S_a) dS_a \tag{15}$$

where $E(P) = \sqrt{\frac{M_4}{M_2}}$ represents the peak crossing rate of the one-sided PSD function of the stress response, and C and m are the material constants of the power-function expression of the S-N curve of the material.

The input load is described by the PSD function, the stress response PSD function of the structure is obtained via frequency response calculation and modal analysis of the system, and the fatigue life of the system is calculated according to the fatigue failure model and the fatigue properties of the material.

4.3.2. Fatigue Analysis

To calculate the stress response spectrum, it is necessary to solve the frequency response function from frame vibration to motor stress based on the finite element model of the motor established in Section 4.1. In this case, unit vertical, lateral, and longitudinal accelerations at each frequency are applied to the bolt hole, and the corresponding frequency response functions are solved separately, as shown in Figure 11.

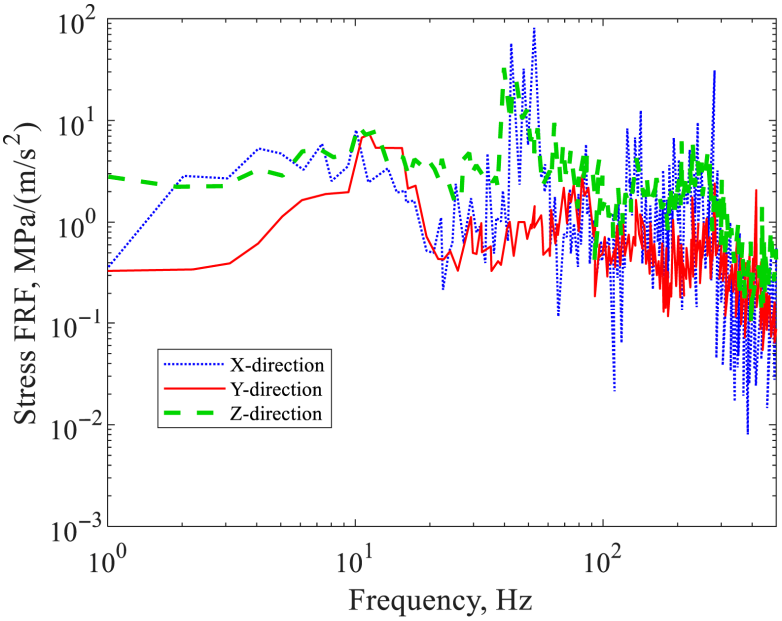


Figure 11. Frequency response functions of bogie frame vibration to equipment stress.

The obtained stress spectra of the bogie motor at operating speeds of 300, 350, 380, 400 km/h, and IEC 61373 were analyzed. The rainflow counting method was used to determine the stress amplitudes and cycles, as shown in Figure 12.

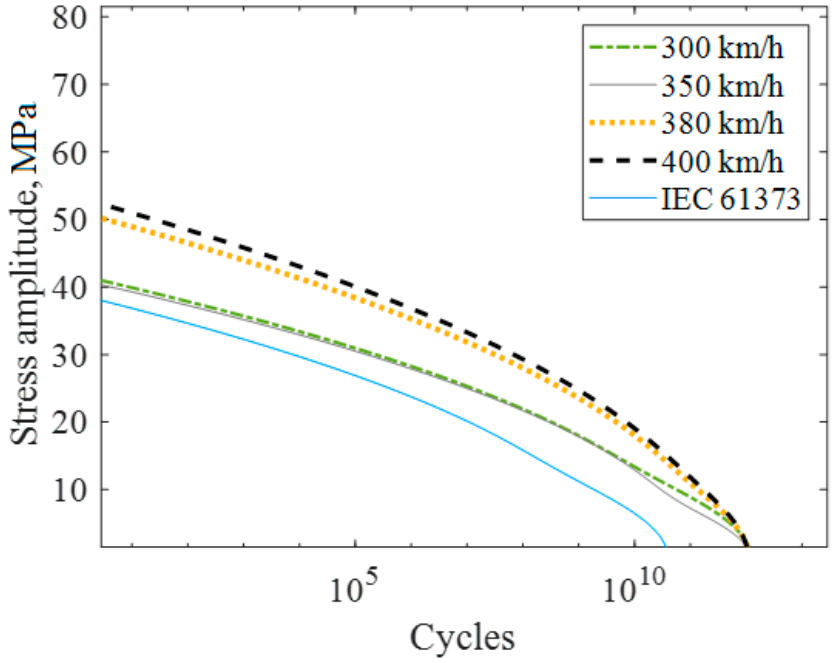


Figure 12. Rainflow counting results for the obtained stress spectra.

With a small number of cycles, the stress amplitude increased from 41.1 to 79.4 MPa as the operating speed increased. At a low stress amplitude, the number of cycles required to reach the fatigue limit increased as the operating speed increased. The stress amplitude was higher than the results obtained based on the IEC61373 standard.

Based on the data obtained using the rainflow counting method, the fatigue damage of the bogie frame mounting seat at different speeds was determined, as shown in Figure 13.

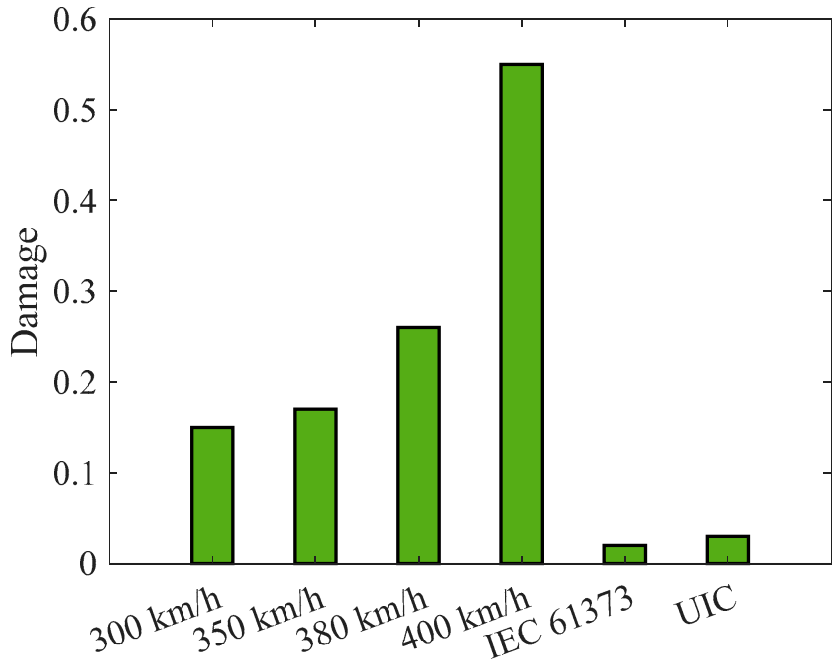


Figure 13. Fatigue damage of the traction motor.

With the increase in operating speed, the fatigue damage increased exponentially. The maximum damage (0.73) occurred at 450 km/h, namely, <1.0, i.e., within the safe range.

From Figure 13, it can be seen that the fatigue damage of the traction motor obtained with the generated vibration spectra is larger than that from the loads defined in the standards. This finding is the result of the generated vibration environment spectrum exhibiting a peak in the 50–60 Hz frequency band, which is consistent with the peak frequency of the FRFs of the traction motor, as shown in Figure 11, meaning that the excitation generated by frame vibration may resonate with the motor mode. This resonance characteristic cannot be achieved by the standard spectrum, reflecting the superiority of the generated spectra.

5. Conclusions

In the study presented herein, a fatigue analysis of the bogie frame and mounted traction motor of a high-speed train was performed. A meticulously designed on-site testing method was used to accurately determine the dynamic stress of the bogie frame, and the result is more accurate than the dynamic stress values obtained using existing numerical methods. The fatigue damage of the bogie frame increases linearly with speed. The weak location of the maximum fatigue damage to the bogie frame is the weld at the traction motor seat, whose equivalent stress is 41.4 MPa.

A spectrum synthesis method for the multichannel vibration data of the mounting position of traction power is proposed, which provides a novel method for generating the vibration load spectrum of vehicle structures. The generated vibration spectra can characterize vibration characteristics in the frequency domain of the mounting position of the traction motor, thus effectively analyzing motor fatigue damage compared with the vibration spectra defined in the IEC 61373 standard and the vibration level of the motor defined in the UIC 615-4 standard.

The peak frequency of FRFs is consistent with peaks of the vibration spectra for the traction motor, which causes significant fatigue damage. Moreover, the fatigue damage of the mounted traction motor increases exponentially with increasing speed.

Author Contributions: L.G.: Conceptualization, Methodology, Writing—Original Draft, Funding Acquisition; G.L.: Conceptualization, Data Curation, Formal Analysis, Software; C.C.: Visualization, Investigation, Validation, Experiments; Y.Z.: Resources, Validation, Experiments; H.Z.: Supervision, Writing—Review & Editing; D.G.: Conceptualization, Writing—Review & Editing. All authors have read and agreed to the published version of the manuscript.

Funding: The authors gratefully acknowledge the financial support provided by the major Project of China Academy of Railway Sciences Group Co., Ltd.: 2024YJ085, the Project of Science and Technology Research and Development Program of China National Railway Group Co., Ltd.: Q2024J012.

Data Availability Statement: The datasets used and/or analyzed during the current study are available from the corresponding author upon reasonable request.

Conflicts of Interest: Authors Lirong Guo, Guoshun Li, Can Chen, Yichao Zhang, and Hongwei Zhang, are employed by Locomotive & Car Research Institute, China Academy of Railway Sciences Corporation Limited. The authors declare that the research was conducted in the absence of any commercial or financial relationships that could be construed as a potential conflict of interest.

References

1. Kim, J.S.; Kim, N.P. A study on strength evaluation procedure for the welded bogie frame of tilting railway vehicles. *Int. J. Veh. Des.* **2007**, *43*, 31–48. [CrossRef]
2. Seo, J.-W.; Hur, H.-M.; Jun, H.-K.; Kwon, S.-J.; Lee, D.-H. Fatigue Design Evaluation of Railway Bogie with Full-Scale Fatigue Test. *Adv. Mater. Sci. Eng.* **2017**, *2017*, 5656497. [CrossRef]
3. Kraus, V.; Kepka, M., Jr.; Doubrava, D.; Chvojan, J. Strength Analysis of Tramway Bogie Frame. In *Mechanical Fatigue of Metals: Experimental and Simulation Perspectives*; Springer: Cham, Switzerland, 2019; pp. 327–334.
4. Ji, C.; Sun, S.; Li, Q.; Wang, W.; Ren, Z.; Yang, G. A novel method for the general application of measured load spectra to different high-speed train bogie frames based on virtual track irregularity. *Measurement* **2022**, *198*, 111369. [CrossRef]
5. Yang, Y.; Liu, C.; Chen, L.; Zhang, X. Phase deviation of semi-active suspension control and its compensation with inertial suspension. *Acta Mech. Sin.* **2024**, *40*, 523367. [CrossRef]
6. Yamazaki, Y.; Fujimoto, T.; Shimokawa, Y.; Minami, H.; Kondo, O.; Iokibe, G.; Nakagawa, J. Development of fatigue prediction system for bogie frame using a dynamic analysis model based on high-speed and high-precision stress estimation method. *Electr. Eng. Jpn.* **2024**, *217*, e23469. [CrossRef]
7. Han, Y.; Crosbee, D.; Allen, P.; Feng, W.; Wang, R.; Yu, J. Dynamic fatigue damage calculation for a high-speed train bogie frame considering the three-dimensional gear meshing. *Veh. Syst. Dyn.* **2024**. [CrossRef]
8. Sanikhani, S.A.; Soroush, M.; Kiani, K.A.; Ravandi, M.; Akbarzadeh, M.R. Probabilistic machine learning approach to reliability analysis of a bogie frame under dynamic loading. *Int. J. Rail Transp.* **2024**, *12*, 958–978. [CrossRef]
9. Sun, Y.; Wei, L.; Liu, C.; Dai, H.; Qu, S.; Zhao, W. Dynamic stress analysis of a metro bogie due to wheel out-of-roundness based on multibody dynamics algorithm. *Eng. Fail. Anal.* **2022**, *134*, 106051. [CrossRef]
10. Wang, Q.; Zhou, J.; Gong, D.; Wang, T.; Sun, Y. Fatigue life assessment method of bogie frame with time-domain extrapolation for dynamic stress based on extreme value theory. *Mech. Syst. Signal Process.* **2021**, *159*, 107829. [CrossRef]
11. Wang, T.; Sun, W.; Wang, Q.; Zhang, Z.; He, Y.; Zhou, J. Generation of vibration load spectrum for fatigue analysis of equipment mounted on bogie frame of railway vehicle based on fatigue damage spectrum. *Proc. Inst. Mech. Eng. Part F J. Rail Rapid Transit* **2023**, *237*, 1082–1093. [CrossRef]
12. Roux, C.; Lorang, X.; Maitournam, H.; Nguyen-Tajan, M.L. Fatigue design of railway wheels: A probabilistic approach. *Fatigue Fract. Eng. Mater. Struct.* **2014**, *37*, 1136–1145. [CrossRef]
13. Gong, D.; Shen, Y.; Liu, G.; Wang, Z.; Deng, X.; Sun, W.; Wang, Q.; Wang, T.; Ji, Y.; Zhou, K.; et al. Frequency veering between car body and under-chassis equipment of railway vehicles in vertical bending mode. *Mech. Syst. Signal Process.* **2023**, *185*, 109768.
14. Yuan, Z.; Chen, X.; Li, C.; Ma, L.; Li, Q.; Sun, S.; Wei, Y. The influence of operation variables on stress spectrum of high-speed train bogie frames. *Veh. Syst. Dyn.* **2023**, *61*, 499–512. [CrossRef]
15. Esderts, A.; Willen, J.; Kassner, M. Fatigue strength analysis of welded joints in closed steel sections in rail vehicles. *Int. J. Fatigue* **2012**, *34*, 112–121. [CrossRef]
16. Wang, Z.; Gong, D.; Zhou, J. Mechanism and countermeasure of polygon development of metro wheels under fluctuating wheel-rail normal force. *Mech. Based Des. Struct. Mach.* **2025**. [CrossRef]
17. Li, F.; Wu, H.; Wu, P. Vibration fatigue dynamic stress simulation under non-stationary state. *Mech. Syst. Signal Process.* **2021**, *146*, 107006. [CrossRef]

18. Wang, Z.; Gong, D. A survey on countermeasures of railway vehicle stability decrease caused by the evolution of hollow-worn wheels. *J. Vib. Control.* **2025**, *31*, 864–877. [CrossRef]
19. *IEC 61373*; International Electro Technical Commission Technical Committee 9. Railway Applications-Rolling Stock Equipment Shock and Vibration Test. Standards Press of International Electro Technical Commission: Geneva, Switzerland, 2010.
20. Mu, L.; Huang, H.; Zhang, J.; Cui, X. Data processing and generalization of vibration environment spectra of on-board materials. *Equip. Environ. Eng.* **2010**, *7*, 75–77+88.
21. Zhang, Y.; Li, Y.; Liu, S. Vibration analysis of IEC 61373 standard based on measured data. In Proceedings of the 2021 7th International Symposium on Mechatronics and Industrial Informatics (ISMII), Zhuhai, China, 22–24 January2021.
22. Jang, J.; Park, J.-W. Simplified Vibration PSD Synthesis Method for MIL-STD-810. *Appl. Sci.* **2020**, *10*, 458. [CrossRef]
23. *UIC 615-4*; Powered Vehicles-Bogies and Running Gear-Strength Tests of Bogie Frames. International Union of Railways: Paris, France, 2003.
24. Tao, G.; Liu, Z.; Ji, C.; Yang, G. Establishment and Analysis of Load Spectrum for Bogie Frame of High-Speed Train at 400 km/h Speed Level. *Machines* **2024**, *12*, 382. [CrossRef]
25. Nieminen, V.; Tuohineva, A.; Autio, M. Wheel load reconstruction using strain gauge measurements on the bogie frame for strain prediction and fatigue assessment. *Int. J. Fatigue* **2023**, *170*, 107533. [CrossRef]
26. Deng, C.; Zhou, J.; Sun, W.; Gong, D.; Sun, Y. Analysis of the spectral induction and hierarchical transmissibility for railway vehicles' measurement vibration environment. *Veh. Syst. Dyn.* **2020**, *59*, 1587–1606. [CrossRef]
27. *GT2014-26257*; An Illustration of the Concepts of Verification and Validation in Computational Solid Mechanics. American Society of Mechanical Engineers (ASME): New York, NY, USA, 2012.
28. Dirlik, T. *Application of Computers in Fatigue Analysis*; Warwick University: Coventry, UK, 1985.

Disclaimer/Publisher's Note: The statements, opinions and data contained in all publications are solely those of the individual author(s) and contributor(s) and not of MDPI and/or the editor(s). MDPI and/or the editor(s) disclaim responsibility for any injury to people or property resulting from any ideas, methods, instructions or products referred to in the content.